Conjugated polyelectrolyte (CPE) poly{3-[6-(*N*-methylimidazolium)hexyl]-2,5-thiophene} complexed with DNA — Relation between colloidal level solution structure and chromic effects

Matti Knaapila,[1,] Telma Costa,[2] Vasil M. Garamus,[3] Mario Kraft,[4] Markus Drechsler,[5] Ullrich Scherf,[4] and Hugh D. Burrows[2]*

[1] Physics Department, Institute for Energy Technology, NO-2027 Kjeller, Norway. [2] Department of Chemistry and Coimbra Chemistry Centre, University of Coimbra, 3004-535 Coimbra, Portugal, [3] Helmholz-Zentrum Geesthacht: Zentrum für Material- und Küstenforschung GmbH D-21502 Geesthacht, Germany, [4] Macromolecular Chemistry Group, Bergische University of Wuppertal, D-42119 Wuppertal, Germany, [5] Laboratory for Soft Matter Electron Microscopy, University of Bayreuth, D-95440 Bayreuth, Germany

Running Title: Polythiophene with DNA

*Corresponding author. E-mail: matti.knaapila@ife.no

ABSTRACT: We report on the solution structure and colorimetric changes for ~1 % (w/w) aqueous cationic conjugated polyelectrolyte, poly[3-[6-(N-methylimidazolium)hexyl]-2,5-thiophene] bromide (P3ImiHT), mixed with double stranded (anionic) DNA — P3ImiHT(DNA)$_x$, where x is the molar ratio of DNA base pair to polymer repeat unit. Small-angle X-ray scattering (SAXS) indicate that P3ImiHT forms loose arrays of rodlike chains involving electrostatic repulsion. SAXS and transmission electron microscopy indicate that the DNA addition reduces this repulsion and leads to networks of ~10 nm sized aggregates $\left(x < 0.5 \text{ or } 1.3 < x \le 2.4\right)$; or compact submicron sized particles with rough surface and ~2 nm thick rodlike chains $\left(0.5 \le x \le 1.3\right)$.The absorption spectra red-shift from 440 nm $\left(x < 0.5\right)$ to 510 nm $\left(x \ge 0.5\right)$ on increasing x, indicating an increased chain planarity and conjugation length concomitant with the rodlike segments. The photoluminescence maxima blue-shift from 680 nm $\left(x = 0\right)$ to 661 nm $\left(x = 0.5\right)$ and 628 nm $\left(x = 2.44\right)$, indicating a decrease in interchain interactions. 16-fold dilution does not change the solution structure but reduces interchain energy transfer.

Keywords: conjugated polymers; polythiophenes; DNA; sensing; SAXS

Introduction

Π-conjugated polymers manifest a rich diversity of supramolecular assemblies built through non-covalent bonds.[1] The specificity in molecular interactions, high luminescence of the π-conjugated backbone and the high sensitivity to changes both in its structure and charge distribution, make these materials ideal for chemical sensing.[2, 3] Π-conjugated polyelectrolytes (CPEs) have a large density of charged groups usually incorporated into the terminal position of side chains leading to two major consequences.[4, 5] First, the charged groups can manifest diversity of supramolecular interactions through charge transfer[6, 7] — which can be combined with hydrogen bonds[8, 9] or polar nonpolar effects[10-12], for example. Second, they allow tuning of the solubility in water. This allows their use beyond the supramolecular level, for example in nanostructured silica hybrid materials[13] and in thin films prepared through layer-by-layer techniques.[14] Combination of (1) charge transfer as a molecular probe; and (2) water as a non-noxious environment for biomolecules, makes CPEs attractive not only for chemosensors but also for biosensors[15-18] and protein inactivation.[19]

Much of CPE research in biosensors has involved the cationic tetraalkyl-ammonium group which is particularly successful in interrogating negatively charged DNA phosphate linkages.[20, 21] Bazan and co-workers used trimethyl-ammonium containing polyfluorene and demonstrated a concept where specific DNA complementary peptide nucleic acid (PNA) prevents CPE-DNA interaction, thus allowing the use of this polymers optical signal with and without DNA interaction for DNA sensing.[22] Since its introduction, this idea has been expanded for other properties and more complicated materials using the cationic tetra-alkylammonium group. Al Attar, Monkman, Monteserin and others have fine-tuned CPE-DNA interactions by surfactants[23, 24] while Inganäs and co-workers detailed properties of zwitterionic CPE hydrogels.[25, 26] Burrows and co-workers prepared block copolymers, thus allowing an additional energy transfer between blocks.[27]

However, in addition to these trimethyl ammonium substituted materials, an increasing attention has been paid to the cationic imidazolium group through the synthesis of novel imidazolium substituted

CPEs, such as arylenevinylenes where the imidazolium unit is incorporated in the main chain,[28] or polythiophenes incorporating imidazolium unit in the side chain either in copolymers[29] or block copolymers.[30] These materials are water soluble and can be used in polymer silica hybrid materials,[31] multilayers formed from layer-to-layer processes[32] and as cathode interlayers for organic solar cells.[33, 34] Moreover, imidazolium based ionic liquids[35], which can form lamellar structures themselves,[36] can be used to stabilize polythiophenes in electrochemical devices.[37] It is also possible to prepare imidazolium based block copolymers that provide a platform for microphase separated structures.[30]

In a particular example, Leclerc and coworkers[38-40] employed the imidazolium substituted CPE, poly{1-methyl-3-[2-[(4-methyl-3-thienyl)-oxo]ethyl]-1*H*-imidazolium} (Chart 1 **(P1)**), for probing anionic DNA and proteins. They introduced a sensing method based on the molecular recognition driven backbone planarization. The backbone of coil-like polythiophene is planarized when the polymer is complexed with a single-strand DNA (ssDNA), which leads to a red-shifted absorption and quenched intrinsic fluorescence. In contrast, the fluorescence is increased after addition of a matching complementary strand, due to the modification in the delocalization of π-electrons along CPE backbone. This idea has been developed further for protein detection[41] and device environment that can consist of, for example, an array with different DNA probes.[42]

Chart 1. Chemical structures of discussed CPEs.

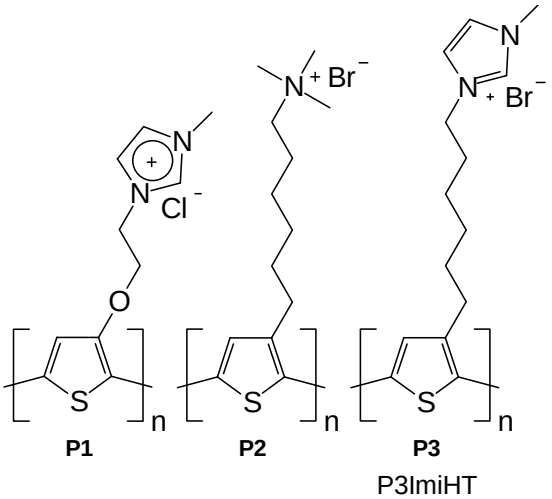

Leclerc and coworkers suggest that the observed interactions occur through self-assembled aggregates, where **P2** is wrapped around the DNA chain. Clearly, the molecular recognition involving interactions between functional groups and the particular CPE conformation at the molecular level must be manifested as large structural effects at the intermolecular or "colloidal" level. While optical data has given the proof of concept for sensing application and detailed insight have been obtained about molecular level interactions, we suggest that understanding its relation to the intermolecular level requires direct structural data. A key methodology here involves small-angle X-ray scattering (SAXS), which has been employed in the studies of DNA,[43] complemented by small-angle neutron scattering (SANS)[44] and light scattering.[45] There is a long and immense tradition for probing proteins and DNA by SAXS.[46, 47] However, in contrast, similar studies of CPE-DNA systems intended for optical sensing seem scarce.

By using combinations of SAXS and SANS, we have recently interrogated the cationic poly[3-(6-trimethylammoniumhexyl) thiophene] (Chart 1, **P2**)[48, 49] and poly[3-[6-(*N*-methylimidazolium)hexyl]-2,5-thiophene] or P3ImiHT (Chart 1, **P3**)[50] complexed with model anionic surfactants, such as sodium dodecylsulfate (SDS). These data provide a quantitative understanding of how "surfactochromic" properties are followed by self-organized structure formation on the intermolecular colloidal scale where this structure has significant differences, which depend on the complexation state.

In this paper, we build upon this understanding towards the relation between optical sensing and intermolecular structural level in CPE – DNA systems. Therefore, we consider combined imidazolium substituted P3ImiHT (**P3**) and double stranded DNA to form P3ImiHT(DNA)$_x$, where x is the molar ratio of DNA base pair to polymer repeat unit. We report on comprehensive SAXS and optical data, and find that aqueous P3ImiHT forms charged rodlike aggregates with interparticle order, which is eliminated by dilution or DNA addition. With increasing DNA content we observe overlapping networks that appear as ellipsoidal $(0.5 < x)$ and rodlike particles $(0.5 \le x \le 1.3)$ at the nanometer level.

Structural transitions lead to concomitant red-shifts in absorption from ca. 440 nm $(x < 0.5)$ to ca. 510 nm $(x \geq 0.5)$, indicating backbone planarization and increased conjugation with the occurrence of rodlike segments. The photoluminescence (PL) maxima are blue-shifted with increasing *x* and with decreasing polymer concentration, indicating a decrease in polymer-polymer interactions. In contrast, the dilution does not influence the solution structure at the colloidal level. These observations provide fundamental information on how DNA complexation is related to the solution structure alongside the chromic response of a water-soluble polythiophene and provide a starting point for the structural studies of three-compound sensory systems.

Experimental

Materials. The synthesis of P3ImiHT **(P3)** via post-polymerization functionalization has been described earlier.[51, 50] The number- and weight-average molecular weights of the precursor polymer P3BrHT were 11.5 kg/mol and 13 kg/mol (the degree of polymerization is about 47). Double stranded DNA lot # BCBK2089V with about 2000 base pairs (average 660 Daltons) was obtained from Sigma-Aldrich. P3ImiHT (10.10 mg/mL) and DNA (5 mg/mL) were mixed with water separately and stirred overnight. These mixtures were mixed to prepare aqueous P3ImiHT(DNA)$_x$, where *x* is the molar ratio of DNA base pairs to monomer repeats. The samples were denoted as S1-S9 and their concentrations and molar ratios are compiled in Table 1.

Additional dilution series were prepared by diluting these samples by the factors of 2, 4, 8 and 16, denoted as S1D1, S1D2, S1D3, S1D4, …, S9D4 respectively. In water, P3ImiHT appears as a transparent solution, while both DNA and P3ImiHT(DNA)$_x$ may contain precipitates. In order to remove possible precipitates, all samples were centrifuged at 10,000 rpm for 2 minutes prior to measurements.

Table 1. Composition of P3ImiHT and P3ImiHT(DNA)$_x$ samples

Sample		*x*	P3ImiHT conc. (mg/mL	DNA conc. (mg/mL)	Total conc. (mg/mL)
S1	P3ImiHT	-	10.10	0.00	10.10
S2	P3ImiHT(DNA)x	0.025	9.18	0.45	9.64
S3	P3ImiHT(DNA)x	0.050	8.42	0.83	9.25
S4	P3ImiHT(DNA)x	0.123	6.73	1.67	8.40
S5	P3ImiHT(DNA)x	0.246	5.05	2.50	7.55
S6	P3ImiHT(DNA)x	0.492	3.37	3.33	6.70
S7	P3ImiHT(DNA)x	1.299	1.68	4.17	5.85
S8	P3ImiHT(DNA)x	2.458	0.92	4.55	5.46
S9	DNA			5.00	5.00

SAXS. SAXS experiments were performed at the BioSAXS Beamline P12 at PETRA III (EMBL/DESY) in Germany. The energy of X-ray beam was 12.8 keV and the beam size 100 (V) μm × 200 (H) μm. Sample to detector distance was 4.1 m and the q-range 0.007 to 0.46 Å^{-1}, as calibrated using diffraction patterns of silver behenate.[52] Scattering patterns were measured using Pilatus 2M pixel detector. The samples (of approximately 20 μL volume) were injected into the sample cuvette using an automated liquid handling sample changer. In order to reduce the risk of radiation damage, the sample was moved slightly during the exposure. The measurement temperature was 20 °C.

For each measurement, 20 diffraction patterns originating from the same sample volume were recorded, using an exposure time of 0.05 s. Before and after each measurement, a signal from pure buffer was measured, and used for background subtraction. The background-corrected data were used to calculate one-dimensional scattering curves by angular averaging. These data were corrected for transmission and incident beam.

In order to verify that no artifacts had occurred as a result of radiation damage, all scattering curves for a recorded dataset were compared to a reference curve (the first exposure) before being integrated using an automated acquisition and analysis program.[53]

The data were analyzed using scaling concepts, where the scattering intensity scales as $q^{-\alpha}$. The exponent $\alpha=1$ refers to separated rodlike or cylindrical particles and $\alpha=2$ to sheet-like particles. The exponent $\alpha=4$ would point to the 3-dimensional particles with a smooth surface. This interpretation was enhanced using the indirect Fourier transformation (IFT) program GNOM.[54] This allowed the evaluation of particle shape in terms of simulated annealing with the program DAMMIF.[55] When the data indicated rodlike particles, the fitting was also conducted to the separate model objects according to the method of Pedersen and Schurtenberger.[56] This analysis gives an idea of possible particle sizes within the selected consideration window.

Cryo-TEM. Electron microcopy was conducted …

Absorption and steady-state fluorescence. The absorption spectra were recorded on a Shimadzu UV-2450 spectrophotometer. The photoluminescence (PL) emission and excitation spectra were recorded with a Horiba−Jobin−Ivon SPEX Fluorog 3-22 spectrometer with the excitation wavelength 450 nm.

The Fluorolog consisted of a modular spectrofluorimeter with double-grating excitation (200−950 nm range, optimized in the UV with a blaze angle at 330 nm) and emission (200−950 nm range, optimized in the visible and with a blaze angle at 500 nm) monochromators. The bandpass for excitation and emission is 0−15 nm with the wavelength accuracy of ±0.5 nm. The excitation source consisted of an ozone-free 450 W xenon lamp. The employed emission detector was a Hamamatsu R928 photomultiplier cooled with a Products for Research thermoelectric refrigerated chamber (model PC177CE005) with a photodiode as the reference detector.

Results and Discussion

Visual considerations. Figure 1 shows images of aqueous P3ImiHT (S1) on the first row, the first on the left. Also shown are images of aqueous P3ImiHT(DNA)$_x$ with increasing molar ratio, x, from left to right (S2-S8); and all samples with decreasing overall concentrations, from top to bottom (D1-D4). When dissolved in water, pure P3ImiHT (S1) appears visually red becoming gradually deeper and subsequently orange-yellow with increasing x. The turning point is located at $x \approx 0.5$ (S6). As each DNA base pair has two negatively charged phosphate units, while the CPE monomer repeat unit has one positively charged imidazolium unit, the nominal charge compensation is achieved at $x = 0.5$,which is concomitant with the visual color change. These chromic effects indicate that DNA is becoming associated with P3ImiHT, preferentially through charge transfer.

Distinctive color changes from red to yellow,[6, 7] yellow to red[38-40] or red to violet and to yellow[50] have been observed for CPEs upon charge compensation with various counterions. Similar colorimetric effects are observed for P3ImiHT upon surfactant complexation.[50] In this case, the complex structure differs from both pure polymer and surfactant micelles on the nanometer level. Assuming that similar effects exist for P3ImiHT(DNA)$_x$ brought us to carry on structural studies.

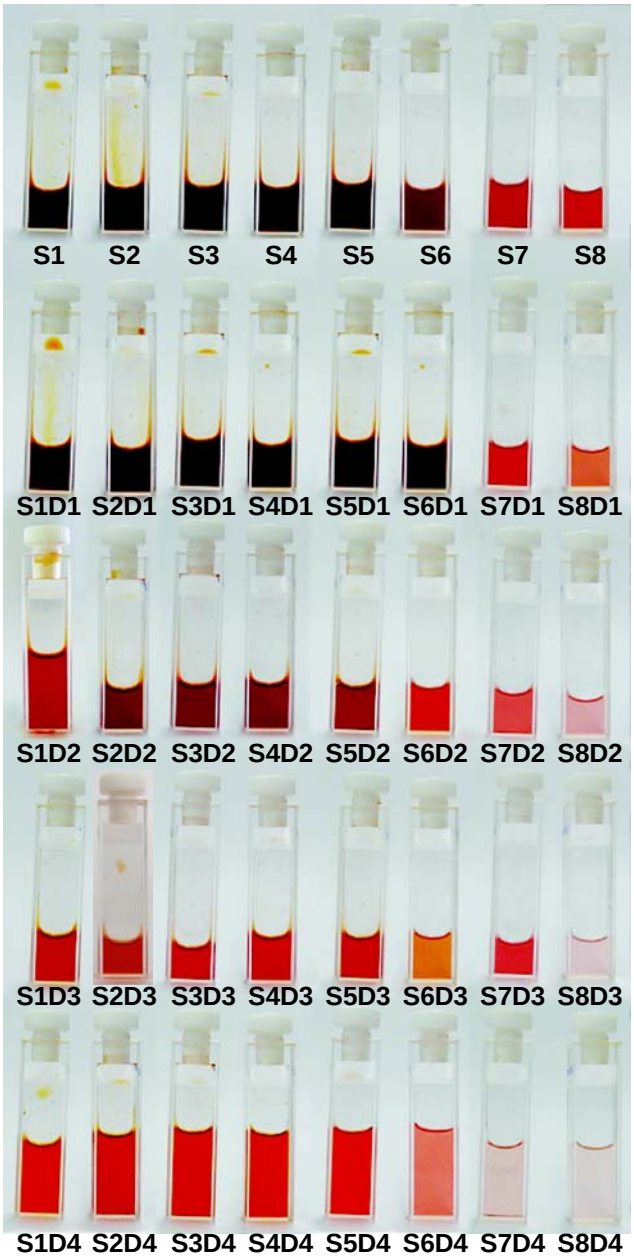

Figure 1. A photo of studied samples and the notation used. From left to right: P3ImiHT (S1) and P3ImiHT(DNA)$_x$ with x≈0.024≈1/40 (S2), 0.049≈1/20 (S3), 0.12≈ 1/8 (S4), 0.24≈1/4 (S5), 0.49≈1/2 (S6), 1.22≈5/4 (S7) and 2.44≈5/2 (S8). Samples from top to bottom correspond to the initial concentrations (Table 1) and the dilutions by the factor of 2, 4, 8 and 16 which are denoted as D1-D4.

Solution structure. *P3ImiHT.* Figure 2 plots the SAXS curves of aqueous P3ImiHT. Essential parameters calculated from the fits to these data are shown in Table 2. The data of aqueous P3ImiHT in our previous work[50] contained a plateau at lower scattering angles, ~0.02-0.03 Å^{-1}, and a broad maximum at higher angles (0.052 Å^{-1} @ 10 mg/mL). These data were interpreted as pointing to interacting charged particles with the radius of gyration $\left(R_g\right)$ of 13.5±0.5 Å.[50] This particle size is comparable to a related polythiophene with longer *N*-methylimidazole terminated side chains showing R_g=16.9 Å.[35]

The current data also show a plateau at ~0.03-0.04 Å^{-1} and a potential maximum that moves towards lower scattering angles with decreasing concentration and (0.063 Å^{-1} @ 10.1 mg/mL and 0.033 Å^{-1} @ 5.05 mg/mL) and vanishes for the lowest concentrations. This move implies a loose order between the polymer particles corresponding to a coherence distance increase from 100 Å to 190 Å. We attribute this effect to the electrostatic repulsion.

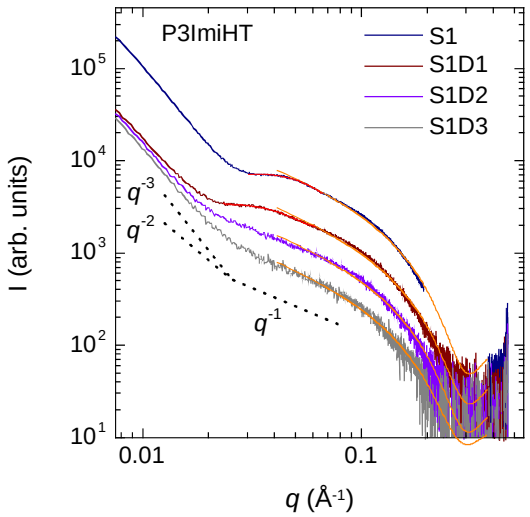

Figure 2. SAXS curves of aqueous P3ImiHT with initial concentration (S1 - blue) and the dilution series D1-D3 (wine, violet and grey). Red and orange lines are fits to the data. Dotted lines show the ideal slopes for comparison.

Table 2. Parameters estimated from the fits to the SAXS data of P3ImiHT[a]

P3ImiHT					
	Conc. (mg/mL)	α		$R_{CS,g}$ (Å)	D_{max} (Å)
		Analysed q-range (Å^{-1})			
		0.0075-0.025	0.025-0.06	0.04-0.37	
S1	10.10	2.76±0.01		8.61±0.01	25
S1D1	5.05	2.05±0.05		8.53±0.01	25
S1D2	2.52	2.30±0.03	0.95±0.01	8.65±0.03	25
S1D3	1.26	2.27±0.02	1.09±0.02	8.85±0.05	25

[a] α is the exponent for a given q-range the scattering intensity scaling as $q\exp(-\alpha)$. $R_{CS,g}$ and D_{max} represent the cross-sectional radius of gyration of and the maximal cross-sectional size of a rodlike scatterer.

With decreasing concentration, the interference maximum disappears and the data begins to follow -1 decay. This indicates emerging rodlike particles, basically locally separated stiff parts of the polymer, and the cross over to Gaussian behavior over longer distances. The deviation from -1 decay at q≈0.027 Å^{-1} gives us an idea of the polymer persistence length ≈ 23 nm. This is illustrated in the Casassa-Holtzer plot shown in the Supporting Information.

The idea of individual chains is in agreement with the thickness (~25 Å) and cross-sectional radius of gyration (~9Å) of stiff objects (Table 2). Thus, the objects appear too thin to accommodate several polymer chains. If this is correct, the broad maximum at higher concentrations would point to the interaction between rodlike parts of the polymers, just masking the -1 decay. The assumption of the same (rodlike) structure is supported by the fact that when the rodlike model is considered, the radius of gyration remains nearly constant, while $I(0)$ scales as polymer concentration. The relative intensities 1070±1, 415.5±0.5, 209.5±0.6 and 106.4±0.6 are obtained for the dilution series S1-S1D3.

Unlike in our previous study,[50] the scattering shows a far more conspicuous upturn at the lowest scattering angles (0.0075-0.025 Å^{-1}). The previous observation window was restricted to 0.01 Å^{-1} and thus the beginning of this upturn was not observable. However, the previous study did not show a significant upturn within the range 0.01-0.025 Å^{-1} either. The degree of polymerization is of the order of 47, which is about twice as much as in our previous work. Assuming that the length of monomer repeat unit along the **c** axis is 4 Å,[57] the polymer length is about 160 Å which is smaller than our observation window (~800 Å). Therefore, should the individual polymers form separated particles of individual coils, this would be visible as a Guiner plateau and not as an upturn.

The upturn follows the decay $\alpha = 2.1 - 2.8$ for 0.0075-0.025 Å^{-1} (Table 2). This scattering may be associated with the mass (or volume) fractal material, where $1 < \alpha < 3$, and stems from loose networks in which the volume and surface have the same fractal dimension.[58] The critical overlap concentration of rodlike macromolecules scales as $1/L^3$, where L is the contour length of the polymer.[59] Even though P3ImiHT would not be strictly rodlike, we can safely assume that increasing polymer length increases probability for their mutual overlap and network formation. Thus, we assume that the polymers are aggregated and that the increasing polymer length leads to network formation, yet not to the precipitation of these aggregates. The SAXS data allows us to probe this system at the nanometer level.

P3ImiHT(DNA)$_x$. Figure 3(a) shows the SAXS curves of aqueous P3ImiHT(DNA)$_x$ at and below the expected charge compensation point ($x \leq 0.5$, S2-S6). The data of P3ImiHT (S1) are shown for comparison. Structural parameters estimated from the fits to the data are compiled in Table 3. The scattering intensity is decreased upon DNA addition. The interference maximum disappears, which is attributed to the vanishing electrostatic repulsion with charge compensation. The particle size increases with DNA addition, which is in agreement with the assumption that P3ImiHT becomes increasingly associated with DNA. In addition, the particles become distinctively rodlike at the charge compensation point.

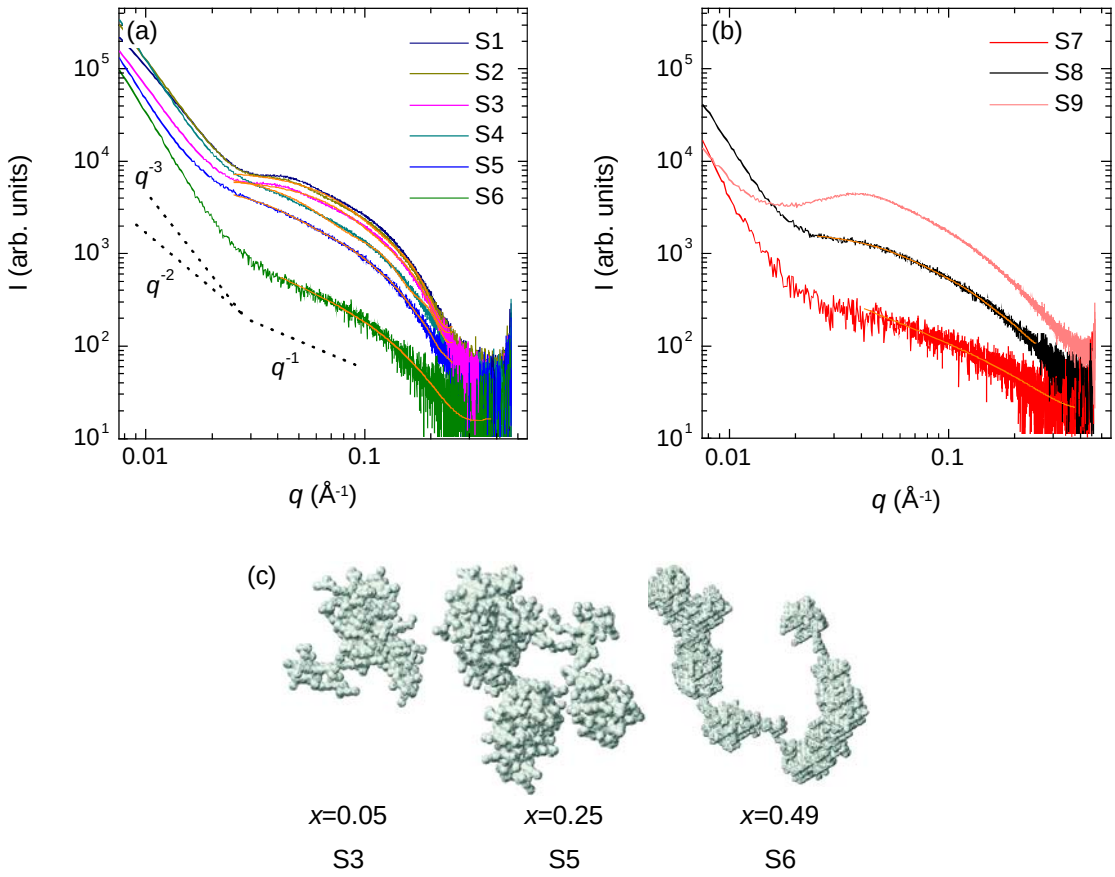

Figure 3. (a) SAXS curves of aqueous P3ImiHT and P3ImiHT(DNA)$_x$ below the assumed charge compensation point (S1-S6 – navy, dark yellow, magenta, dark cyan, blue and olive) and (b) above the assumed charge compensation point (S7-S8 – red, black). The corresponding data of DNA solution is shown for comparison (S9 – salmon). Solid orange lines represent structural models fitted to the data. Dotted black lines show the ideal slopes for comparison. (c) Simulated real space examples obtained from the fits to the data S3, S5 and S6.

A distinctive upturn exist even though all the samples have been centrifuged prior to measurements. For $0.025 \le x \le 0.25$, the scattering power is not consistently below or above 3. For $0.5 \le x \le 1.3$ the scattering power falls within the interval $3 < \alpha < 4$, which is indicative of surface fractal material. Basically, this points to the particle core with an Euclidean dimension $D_v = 3$ and rough surface obeying the surface fractal dimension $D_s = 6 - \alpha$.[58]

Figure 3(b) shows the SAXS curves of aqueous P3ImiHT(DNA)$_x$ above the expected charge compensation point ($x > 0.5$, S7-S8). The data of aqueous DNA (S9) are shown for comparison. The SAXS curves of the DNA dilution series are plotted in the Supporting Information. The corresponding parameters are compiled in Table 3. The particles are rodlike just above the charge compensation point (S7). The scattering intensity increases again, and free DNA becomes visible after further DNA addition (S8). As with P3ImiHT, the scattering power at the lowest q falls between 2 and 3.

The DNA scattering curves correspond to those discussed in Ref.[43] These include a broad scattering maximum moving towards smaller q with decreasing concentration. This shift is due to the electrostatic and excluded volume interactions, and although reported to scale as $conc.^{-1/2}$, our data point to a smaller scaling power.

Figure 3(c) shows real space examples of the local structures, as obtained from the fits to the data by simulated annealing. The models consist of so called dummy atoms whose diameter is 4 Å corresponding to the length of P3ImiHT monomer. They are in agreement with the increase of particle size with increasing x below charge compensation and with the change in the particle shape towards flexible cylinders upon charge compensation.

Table 3. Parameters estimated from the fits to the SAXS data of P3ImiHT(DNA)$_x$.[a]

P3ImiHT(DNA)x								
	x	α		Model		R,g (Å)	R_{CS},g (Å)	Dmax (Å)
		Analysed q-range (Å^{-1})						
		0.0075-0.025	0.025-0.25	0.025-0.25	0.04-0.37			
S2	0.025	3.03±0.02	-	3D object	-	21.09±0.01	-	55
S3	0.050	2.77±0.03	-	3D object	-	20.83±0.01	-	55
S4	0.123	3.26±0.03	-	3D object	-	30.67±0.03	-	80
S5	0.246	2.79±0.05	-	3D object	-	37.33±0.17	-	115
S6	0.492	3.74±0.02	1.36±0.02	-	Cylinder	-	8.57±0.08	25
S7	1.299	3.27±0.09	1.02±0.02	-	Cylinder	-	5.64±0.03	15
S8	2.458	2.82±0.06	-	3D object	-	24.43±0.16	-	80

[a] α is the exponent for given q-range. $R_{,g}$ and $R_{CS,g}$ represent the radius of gyration of 3-dimensional arbitrary shaped scatterer and the cross-sectional radius of gyration or a rodlike scatterer. D_{max} represents corresponding maximal particle size or cross-sectional size.

Figure 4 shows the cryo-TEM images of aqueous P3ImiHT(DNA)$_x$ for $x = 0.05$ and $x = 0.5$. In the submicron scale, the former sample appears as a network of fibrous material (Figure 4(a)) while the latter sample appears as a network of spheres with rough surface (Figure 4(b)). This is in a perfect agreement with SAXS data that indicate volume and surface fractal submicron scaled structures, respectively. This picture concerns mainly larger length scale than seen by SAXS and the observed nanometer scaled 3D and rodlike particles appear within the observed submicron sized arrays. The rodlike particles with the diameter of few nm may be observable in higher magnification for $x = 0.5$ (Figure 4(c)). This observation supports the existence of the rigid segments seen by SAXS data.

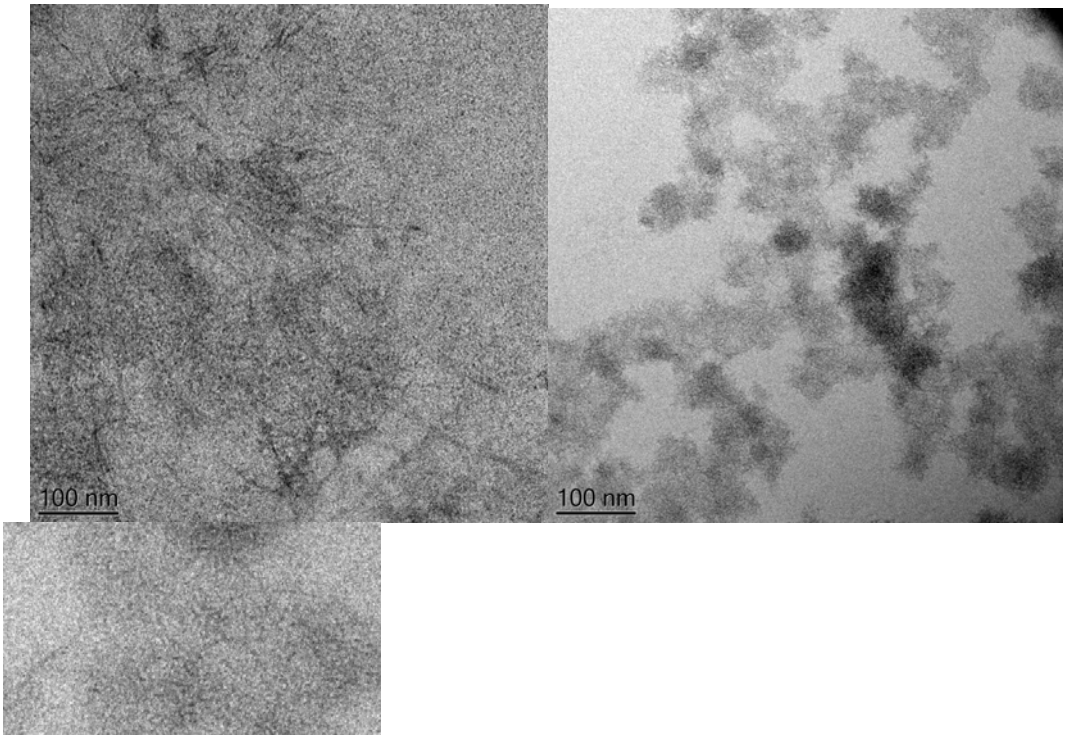

Figure 4. Cryo-TEM images of aqueous P3ImiHT(DNA)$_x$ for (a) $x = 0.05$ (b-c) $x = 0.5$.

DNA effect. The important question arising from these data is to what extent the changes in the scattering patterns are due to the DNA addition and dilution. The amount of material contributing to the scattering curve is not clear since (1) the material has been centrifuged and occasional precipitates removed and (2) larger objects fall outside the observation window. Finally, there is a question of contrast difference. If we assume that the density is 1 g/mL for all constituents, we estimate scattering length densities of $8.64 \cdot 10^{10}$ cm^{-2}, $8.92 \cdot 10^{10}$ cm^{-2} and $9.44 \cdot 10^{10}$ cm^{-2} for P3ImiHT, DNA and water, respectively. This implies that the X-ray contrast P3ImiHT/water is similar to DNA/water and P3ImiHT/DNA basically negligible. Thus, the scattering data of aqueous P3ImiHT(DNA)$_x$ provide information of overall complex and its constituents are not emphasised.

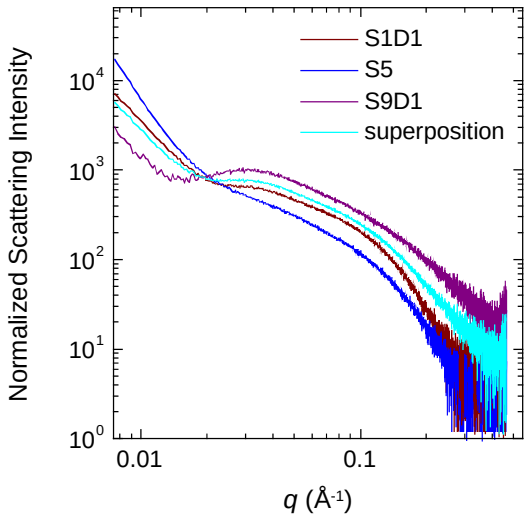

Figure 5. SAXS curves of aqueous P3ImiHT (S1D1 - wine), P3ImiHT(DNA)$_{0.25}$ (S5 - blue) and DNA (S9D1 - purple). Concentrations of pure P3ImiHT and DNA solutions are 5.0 mg/mL and 2.5 mg/mL and the total concentration of P3ImiHT(DNA)$_{0.25}$ is 7.5 mg/mL. Thus, the concentrations of pure compounds are the same as their concentrations in their mixture. Superposition of S1D1 and S9D1 curves is shown for comparison (cyan).

Figure 5 plots the SAXS curves of P3ImiHT, DNA and P3ImiHT(DNA)$_{0.25}$ normalized to the concentration. The overall concentrations are 5.0 mg/mL, 2.5 mg/mL and 7.5 mg/mL. This means that the concentrations of pure compounds are the same as their concentrations in the complex sample. Also shown is the superposition of the pure compounds. All curves are clearly different. This indicates that the scattering differences do not stem from the different concentrations, but must be associated with the DNA interaction.

Aqueous P3ImiHT(DNA)$_{0.25}$ contains small 3D particles and the question is whether they correspond to the coiled molecules or polymer-DNA associations. P3ImiHT(DNA)$_{0.25}$ does not show interference maxima that are visible for P3ImiHT and DNA. This points to the interaction between polymer and DNA at the local nanometer scale, yet the charge mismatch should lead to free P3ImiHT coexisting with P3ImiHT(DNA)$_{0.25}$. P3ImiHT and the superposition curve virtually coincide below 0.02 Å^{-1}. This indicates that the polymer-DNA interaction is not dominant at the submicron level. These observations provide evidence for P3ImiHT and DNA being locally intertwined, as implied by the visual chromic effect. They are also consistent with Leclerc's idea about DNA being wrapped over **P1**.[38-40]

The SAXS curves of the P3ImiHT(DNA)$_x$ dilution series normalized to the overall concentration are shown in the Supporting Information and the curves of dilution series are qualitatively similar for each x. The normalized scattering intensity level may vary slightly for the lowest concentration, but this is attributed to the imprecision of background subtraction in the weakest scattering samples. Similarities in scattering curves imply that the interpretation drawn from one concentration is valid over the studied concentration range (~0.06-1 %).

Packing of cylindrical particles. The SAXS curves scaling as -1 point to the locally separated rodlike particles for P3ImiHT and for P3ImiHT(DNA)$_x$ when crossing over the charge compensation point. The deviation from -1 decay is observed at q≈0.027 Å^{-1}, 0.029 Å^{-1} and 0.017 Å^{-1} for P3ImiHT (S1D3) and P3ImiHT(DNA)$_{0.5}$ (S6) and P3ImiHT(DNA)$_{1.3}$ (S7) as seen in the Casassa-Holtzer plots (Supporting Information). This deviation can represent a cross-over either due to the scattering of larger aggregates

or Gaussian chains. They would correspond to the lowest estimations of polymer persistence lengths ≈ 23 nm, 22 nm and 37 nm.

Figure 6 plots the $p(r)$ functions deduced from the model of rodlike particles for diluted P3ImiHT and for P3ImiHT(DNA)$_{0.5}$ and P3ImiHT(DNA)$_{1.3}$. The distribution of P3ImiHT and P3ImiHT(DNA)$_{0.5}$ are similar, pointing to a 25 Å diameter, while there is a tendency towards thinner 15 Å diameter structures for P3ImiHT(DNA)$_{1.3}$. These values correspond to the hydrodynamic diameter of DNA, 22-26 Å.[60] This implies that, while DNA is clearly increasing the particle size below the charge compensation point, it may not be tightly wrapped around the polymer (or the other way round) at the charge compensation point. Instead, the rigid polymer or DNA sections seen at the nanometer level may remain isolated at least by a thin intercalated water layer or by a side chain layer containing more water than the main chain layer. Based on the differences in persistence lengths and particle diameters, it seems that the samples S6 and S7 represent different structures, S6 possibly pure P3ImiHT and S7 possibly pure DNA.

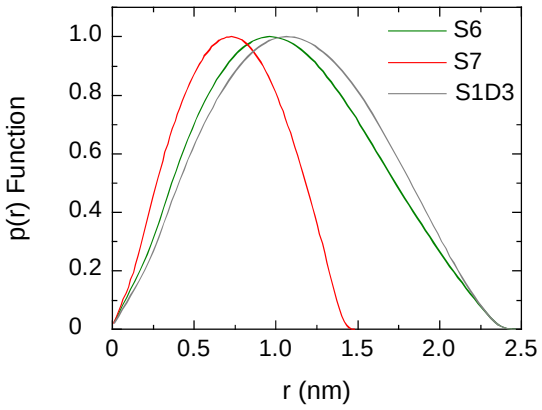

Figure 6. The $p(r)$ functions for P3ImiHT with 8-fold dilution (S1D3 - grey) and P3ImiHT(DNA)$_x$ with $x = 0.5$ (S6 - olive) and 1.3 (S7 - red).

Photophysical consequences. *UV/Visible absorption.* Figure 7(a) shows the normalized absorption spectra of aqueous P3ImiHT and P3ImiHT(DNA)$_x$ for the initial concentration (1 % (w/w)). Figure 7(b) shows the corresponding data after 16-fold dilution. The non-normalized spectra corresponding to the normalized spectra shown in Figure 6(b) as well as the spectra for the full dilution series are shown in the Supporting Information. The spectra of diluted samples are qualitatively similar to those of the initial concentration samples. The non-normalized spectra show how the absorption maximum scales as polymer concentration.

The spectrum of P3ImiHT is characterized by a broad and non-resolved band with a maximum at 436 nm, characteristic of disordered polythiophene derivatives in solution. As expected from the visible color changes of the solutions, the presence of DNA leads to a progressive red-shift of the absorption maxima $\left(\lambda_{\text{abs}}^{\max}\right)$ and the absorption band becomes broader at low molar ratios $\left(x \le 0.5\right)$. Even though the SAXS interference maximum disappears, implying to the close contacts of oppositely charged P3ImiHT and DNA, the broader absorption spectra implies coexistence of free P3ImiHT and P3ImiHT(DNA)$_x$ complexes. For $x > 1.3$, the red-shifted absorption spectra become narrower again with a $\lambda_{\text{abs}}^{\max} = 509$ nm. Figure 7(c) plots the observed maxima in the absorption spectra with increasing *x*. Also shown is the shift relative to the pure polymer $\left(\Delta\lambda\right)$.

We expect that the red-shift is related to a conformational change of the π-conjugated backbone from a distorted conformation of the aqueous P3ImiHT solution to a more planar and more conjugated backbone for P3ImiHT(DNA)$_x$. The idea of backbone planarization is consistent with the emerging rodlike segments observed in the SAXS data and may stem from the Coulomb interactions that drive P3ImiHT chains increasingly oriented along DNA chains. Previous studies on structurally related polythiophene-ssDNA based CPE-CPE complexes revealed that the shifts in the absorption spectra are related to the formation of a duplex between polythiophene based CPE and ssDNA, resulting in a change of the backbone conformation.[61]

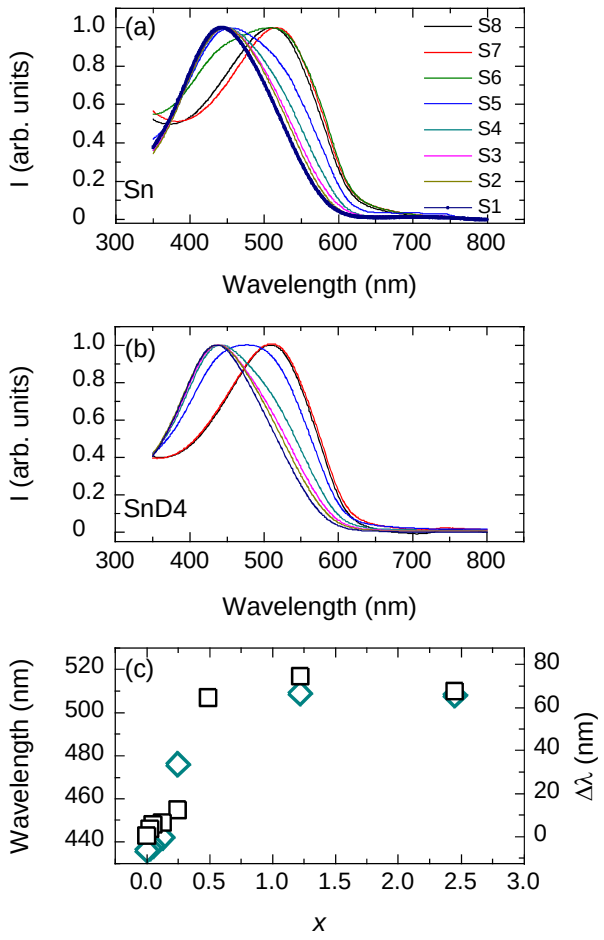

Figure 7. Normalized absorption spectra of aqueous P3ImiHT(DNA)$_x$ with increasing x. (a) Initial concentration (Sn) and (b) 16-fold dilution (SnD4) (S1-S8 - navy, dark yellow, magenta, cyan, blue, olive, red and black). (c) The absorption maxima and the shift relative to the pure polymer spectrum with increasing x for the initial concentration (black squares) and 16-fold dilution (cyan diamonds).

Photoluminescence. Figures 8(a) and 8(b) show the PL spectra of aqueous P3ImiHT(DNA)$_x$ mixtures for the initial concentration (~1 % (w/w)) and for the 16-fold dilution. Changes in the PL maxima with increasing *x* are plotted in Figure 7(c). The non-normalized PL spectra and the full dilution series are shown in the Supporting Information. Considering the initially prepared higher concentration samples, the PL spectra for P3ImiHT consist of a broad and featureless band with maximum at 680 nm. Again, the presence of DNA induces shifts of the peak maxima $\left(\lambda_{\mathrm{em}}^{\max}\right)$. For $x < 0.5$, $\lambda_{\mathrm{em}}^{\max}$ slightly blue-shifts to 661 nm. For $x \geq 0.5$, a further blue-shift to 628 nm is observed. Absorption and PL spectra reflect a distinct decrease of the Stokes shift for P3ImiHT(DNA)$_x$. The PL properties of P3ImiHT(DNA)$_x$ are changed with 16-fold dilution. First, the PL maximum at 636 nm $\left(x = 0\right)$ slightly red-shifts by 12 nm to 648 nm $\left(x = 0.5\right)$. For $x \geq 0.5$, the PL maxima are shifted in the opposite direction to ca. 610 nm, similar, but not identical, to what is observed for the higher concentration sample.The PL spectra of both series display a vibrational structure near the charge compensation point, e.g. for samples S7 $\left(x = 1.25\right)$ and S6D4 $\left(x = 0.5\right)$. For these samples two maximum wavelengths were identified and plotted in Figure 8(c). Blue-shifts in PL spectra are commonly found for CPE-surfactant systems.[10, 63] Next, we pay attention on the slight red-shift observed for $x = 0 - 0.5$.

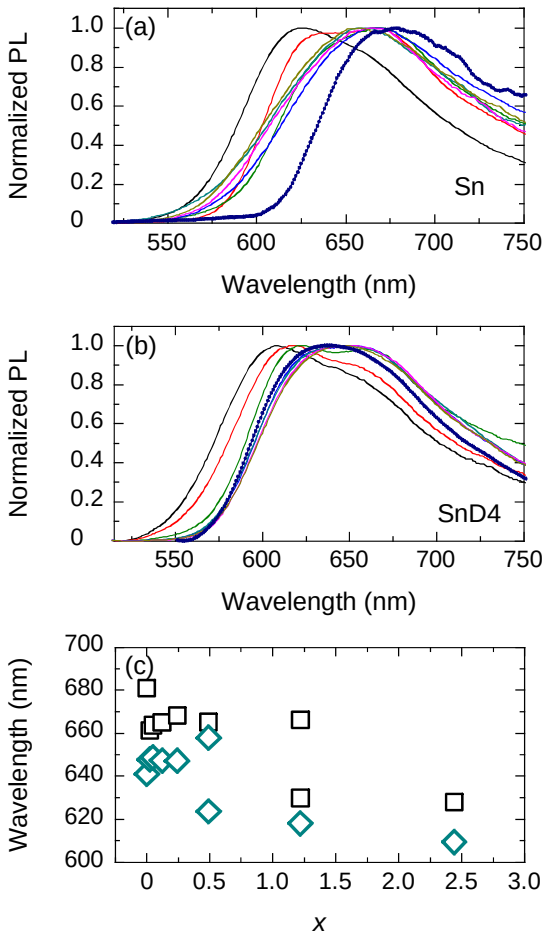

Figure 8. Normalized PL spectra of aqueous P3ImiHT(DNA)$_x$ with increasing x. (a) Initial concentration (Sn) and (b) 16-fold dilution (SnD4) (S1-S8 - navy, dark yellow, magenta, cyan, blue, olive, red and black). (c) The PL maxima with increasing x for the initial concentration (black squares) and 16-fold dilution (cyan diamonds).

Two main effects may contribute to the PL shifts. First, the twists and kinks along the polymer lead to an inhomogeneous distribution of subunits with different conjugation lengths, which result in the lower energy sites to where the photoexcitation energy can migrate. The increase of the conjugation length leads to an increase in the maximum emission wavelength and the PL spectra are red-shifted. Second, interpolymeric interactions between adjacent polymer chains can create a new energy transfer path. The close contacts between subunits of different polymer chains leads to the migration of photoexcitation energy between subunits. Again a red-shift of the PL spectrum is expected.

We expect that the red-shifted absorption spectra with increasing *x* indicate a greater planarization and an increased conjugation length due to the interaction between P3ImiHT and DNA. Thus, increasing planarization would lead to red-shifted PL spectra with increasing *x*. On the other hand, decreasing P3ImiHT concentration reduces tendency to close polymer-polymer contacts, which limits energy transfer to lower energy-emitting sites and leads to the blue-shifted PL spectra with increasing *x*. We propose that the balance between these two opposing effects explains the subsequent red-shift and blue-shift observed in the PL spectra of diluted P3ImiHT(DNA)$_x$ with increasing *x* (Figures 8(b) and (c)). This idea is also supported by the appearance of vibronic structure at $x = 0.5 - 1.3$, indicating that the interpolymeric interactions become weak. For $x = 2.4$, the PL spectra are blue-shifted and similar for all dilutions, presumably due to the decrease in the polymer-polymer interactions.

The PL spectra of P3ImiHT(DNA)$_x$ depend on the total concentration (sum of P3ImiHT and DNA) while the absorption spectra remain essentially similar. The non-complexed P3ImiHT displays a blue-shift of ca. 42 nm between initial aqueous solution (S1) and 16-fold dilution (S1D4). This shift is consistent with the decreasing polymer-polymer interactions, seen as vanishing interference maximum in SAXS data. For $0.25 < x < 0.5$, the concentration effect is lower and the PL spectra are shifted by only ca. 10 nm upon dilution. In this regime, there is not enough DNA to bind all P3ImiHT but the formation of ground state aggregates involving more than one P3ImiHT chain is possible. This is supported by the broadened absorption spectra, suggesting coexistence of free and complexed P3ImiHT. For $0.5 \le x < 1.22$, the concentration dependence is again significant with the PL shifts of 47-52 nm.

SAXS data do not depend on concentration except for pure P3ImiHT and pure DNA. While increasing concentration leads to the increased probability for chains to touch each other and to the red-shifted PL, this does not influence nanometer scale particle shape and small-angle scattering. In contrast, increasing DNA leads to a different particle shape that becomes visible in the SAXS data.

Photoexcitation profile. Figures 9(a) and 9(b) show the PL excitation profiles of aqueous P3ImiHT(DNA)$_x$ for the initial high concentration and for the 16-fold dilution. The excitation spectra differ from the corresponding absorption spectra (Figure 7), in particular, in the absence of DNA and at low DNA concentration. The excitation spectrum of pure P3ImiHT solution (Figure 9(a)) shows a very sharp band at 590-600 nm. This band present when the interpolymeric interactions are favorable, i.e., at low *x* and at high polymer concentrations and it disappears upon dilution (S1-S1D4) or DNA addition. This indicates that the band is related to P3ImiHT aggregates.

As already mentioned, when the P3ImiHT aggregates are present, the absorption and emission occur from different sites due to electronic energy migration of the excited state. We suggest that this explains significant differences between the absorption and PL excitation spectra and that the PL excitation band thus originates from energetically "relaxed" states near the absorption edge. Support to this idea comes from temperature dependent studies on regioregular poly(3-hexylthiophene) in methylcyclohexane.[64] These studies showed that characteristic absorption band of polythiophenes is replaced with a red-shifted band with decreasing temperature and that the new band at 500-650 nm can be assigned to polymer aggregates.

For $x \leq 0.25$ the excitation spectra are very broad and show peak maxima at 370-400 nm, indicating that the effective conjugation length is interrupted by kinks and twists, suggesting coexistence of free and complexed P3ImiHT chains. For $x \geq 0.5$, the excitation maxima are red-shifted to 480 nm due to the presumably more planar structure and increased effective conjugation length. The spectra become similar to the UV/vis absorption spectra but they are still shifted relative to each another. The red-shift between the absorption and excitation spectra reflects the difference between the absorbing and emitting species in the system, as explained earlier. This effect diminishes with increasing the DNA content in the mixture due to decreased P3ImiHT-P3ImiHT interactions and planarization of the P3ImiHT backbone. When planarization of the P3ImiHT backbone causes a sharpening of the PL excitation spectra, the absorption and excitation spectra become comparable, too. We observed the same effect when P3ImiHT was complexed by an anionic surfactant, SDS.[50]

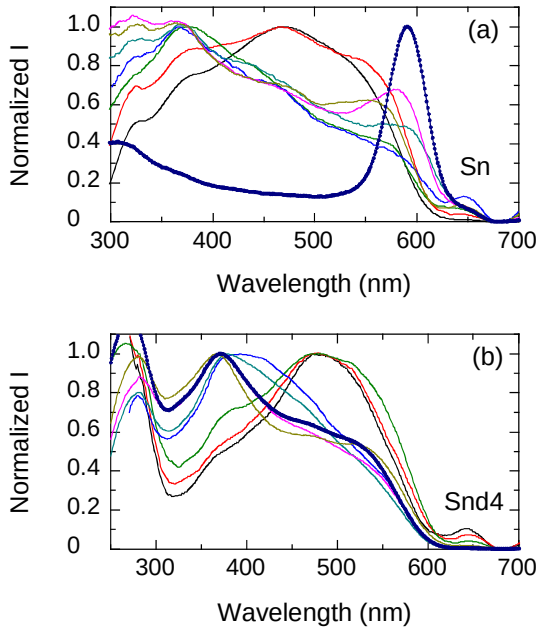

Figure 9. Normalized PL excitation profiles of aqueous P3ImiHT(DNA)$_x$ with increasing x. (a) Initial concentration (Sn) and (b) 16-fold dilution (SnD4) (S1-S8 - navy, dark yellow, magenta, cyan, blue, olive, red and black).

Tentative phase diagram. Figure 10 outlines the tentative structural idea of P3ImiHT and P3ImiHT(DNA)$_x$ with increasing x. This refers to the overall concentration of ~0.06-1 % at room temperature, when any potential precipitates are removed by centrifugation. We may identify six possible phase regimes. (1) Pure P3ImiHT polyelectrolyte (S1). Polymer forms interacting charged particles that merge into loose networks. The particle-particle distance becomes longer and the interaction becomes weaker with decreasing concentration. Locally, separated individual chains are emerging. (2-3) Complexes below the charge compensation point (S2-S5), $x < 0.5$. Particles become larger but the interaction vanishes. Complexes coexist with free P3ImiHT. The scattering intensity decreases and the interaction maximum disappears with increasing x. (4) Crossing over the nominal charge compensation point (S6-S7), $0.5 \le x \le 1.3$. P3ImiHT-DNA associations become rodlike. The scattering intensity reaches its minimum following power $\alpha \approx 1$. No interactions between the chains. (5) Above the charge compensation point (S8) $x > 1.3$. Interactions reappear and finally free DNA becomes visible, the scattering intensity increases again. (6) Pure DNA taking its rodlike structure with the electrostatic repulsion between the chains.

Consistent with the SAXS data, the optical data suggest that DNA induces different conformational changes to the polythiophene backbone with increasing x. P3ImiHT becomes planarized with increasing DNA content, leading to red-shifted absorption for all x and red-shifted PL spectra for $x < 0.5$. Increasing DNA fraction further still or decreasing sample concentration leads to weaker interpolymer interactions and blue-shifted PL spectra.

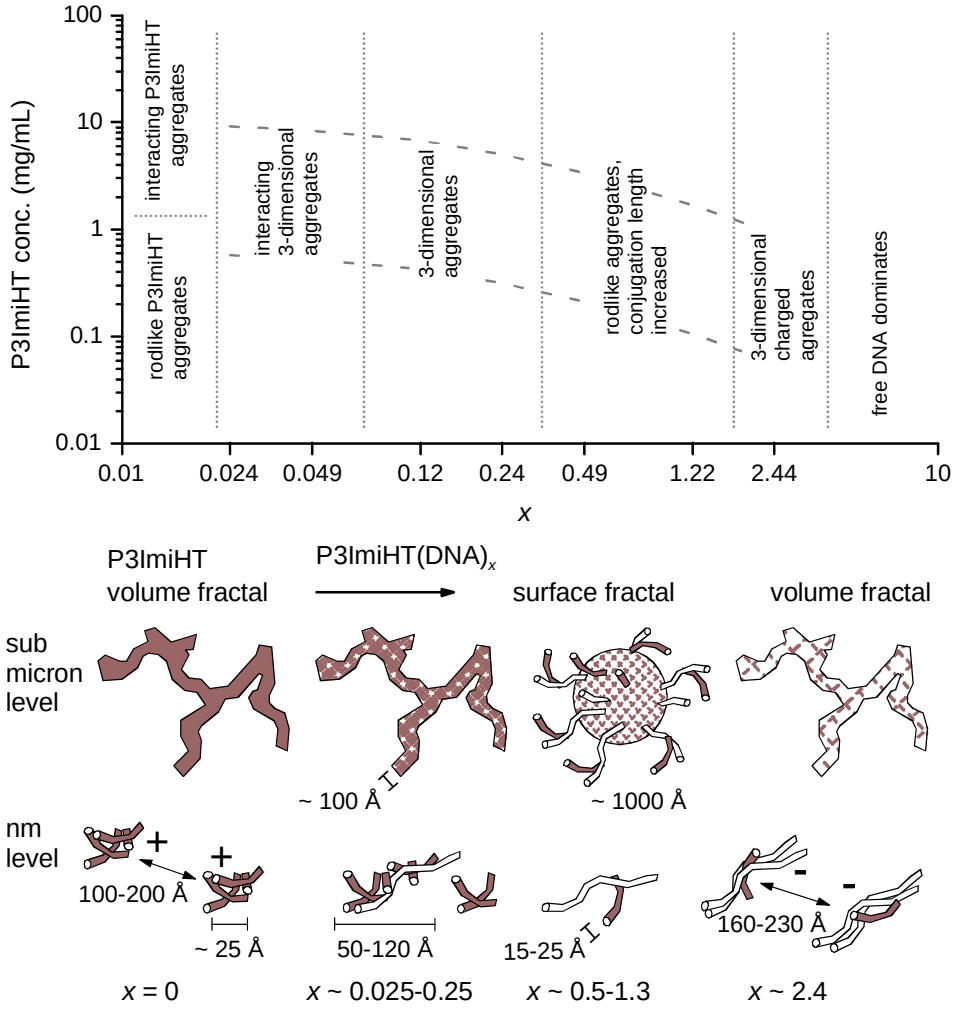

Figure 10. Top: A room temperature phase diagram of aqueous P3ImiHT(DNA)$_x$ as a function of polymer concentration and molar ratio, x. Dotted lines represent phenomenological phase regimes. Dashed lines mark the studied concentration range. Bottom: Illustration of suggested aggregate structures for different x at the submicron and nanometer scales. Terracotta and white represent P3ImiHT and DNA, respectively.

Conclusions

In a 1 % (w/w) aqueous solution the conjugated polyelectrolyte P3ImiHT appears locally as isolated stiff polymers merging to form larger aggregates on the nanometer level. Electrostatic repulsion between the chains leads to the loose intermolecular ordering that disappears upon tenfold dilution or with DNA addition. The solution structure should be discussed at both the nanometer level and at the submicron level. The P3ImiHT(DNA)$_x$ complex appears as ellipsoidal $(x < 0.5)$, rodlike $(0.5 \le x \le 1.3)$ and ellipsoidal particles $(x = 2.4)$ at the nanometer level. Free DNA may be visible for $x > 1.3$. Submicron sized particles with dense core and rough surface (surface fractals) are observed at the charge compensation point $(0.5 \le x \le 1.3)$. Loose submicron sized networks (volume fractals) are observed with excess charges $(x < 0.5$ or $x > 1.3)$.

Structural transitions are concomitant with red-shifts of the absorption maxima from ca. 440 nm $(x < 0.5)$ to ca. 510 nm $(x \ge 0.5)$ indicating a conformational change from a non-planar and distorted to more planar and higher conjugated backbone structure, concomitant with the occurrence of rodlike aggregates. The PL maxima for P3ImiHT(DNA)$_x$ are shifted from 680 nm $(x = 0)$ to 661 nm $(x = 0.5)$ and 628 nm $(x = 2.44)$ indicting a balance of increasing planarization and decreasing polymer-polymer interactions on increasing *x*. 16-fold dilution leads to blue-shifted PL features indicating decreased polymer-polymer interactions, whereas the nanometer level structure is not changed. This stems from the fact that PL spectra detect changes of the backbone conformation as well as short distance interpolymeric interactions. These changes are not necessarily manifested as morphological changes on the nanometer scale.

This work gives one framework for the connection between the solution structure and chromic response of a water-soluble P3ImiHT on DNA complexation. The next step should begin with a single stranded DNA and follow the addition of complementary strand *in situ*. Future work should also focus on the neutron scattering studies and contrast variation to observe structure inside the particles.

Furthermore, the effect of polymer counterion could be clarified using SAXS and heavy ion replacement, as already demonstrated for DNA covered nanoparticles.[65]

Acknowledgement. We thank Clement Blanchet of EMBL for experimental assistance with the SAXS measurements at P12 BioSAXS. T.C. thanks FCT, the Portuguese agency for scientific research, which has supported this work through a Postdoctoral Grant (SFRH/BPD/47181/2008). Financial support of the Coimbra Chemistry Centre from the FCT through project PEst-OE/QUI/UI0313/2014 is gratefully acknowledged

Supporting Information Available. Casassa-Holtzer plots, SAXS curves of the used DNA water solutions as well as additional SAXS curves and the photoabsorption, PL and excitation spectra of P3ImiHT(DNA)$_x$ upon dilution. This material is available free of charge via the Internet at http://pubs.acs.org.

References

(1) Hoeben, F. J. M.; Jonkheijm, P.; Meijer, E. W.; Schennnig, A. P. H. J. *Chem. Rev.* **2005**, 105, 1491-1546.

(2) McQuade, D. T.; Pullen, A. E.; Swager, T. M. *Chem. Rev.* **2000**, 100, 2537-2574.

(3) Rochat, S.; Swager, T. M. *ACS Appl. Mater. Interfaces* **2013**, 5, 4488-4502.

(4) Jiang, H.; Taranekar, P.; Reynolds, J. R.; Schanze, K. S. *Angew. Chem. Int. Ed.* **2009**, 48, 4300-4316.

(5) Liu, B.; Bazan, G. C., *Conjugated Polyeletrolytes - Fundamentals and Applications*. Wiley-VCH: Chichester, 2013.

(6) McCullough, R. D.; Ewbank, P. C.; Loewe, R. S. *J. Am. Chem. Soc.* **1997**, 119, 633-634.

(7) Chen, L.-H.; Xu, S.; McBranch, D.; Whitten, D. *J. Am. Chem. Soc.* **2000**, 122, 9302-9303.

(8) Zanuy, D.; Aleman, C. *J. Phys. Chem. B* **2008**, 112, 3222-3230.

(9) Preat, J.; Teixeira-Dias, B.; Michaux, C.; Perpete, E. A.; Aleman, C. *J. Phys. Chem. A* **2011**, 115, 13642-13648.

(10) Lavigne, J. J.; Broughton, D. L.; Wilson, J. N.; Erdogan, B.; Bunz, U. H. F. *Macromolecules* **2003**, 36, 7409-7412.

(11) Burrows, H. D.; Lobo, V. M. M.; Pina, J.; Ramos, M. L.; de Melo, J. S.; Valente, A. J. M.; Tapia, M. J.; Pradhan, S.; Scherf, U. *Macromolecules* **2004**, 37, 7425-7427.

(12) Burrows, H. D.; Tapia, M. J.; Fonseca, S. M.; Valente, A. J. M.; Lobo, V. M. M.; Justino, L. L. G.; Qiu, S.; Pradhan, S.; Scherf, U.; Chattopadhyay, N.; Knaapila, M.; Garamus, V. M. *ACS Appl. Mater. Interfaces* **2009**, 1, 864-874.

(13) Evans, R. C.; Macedo, A. G.; Pradhan, S.; Scherf, U.; Carlos, L. D.; Burrows, H. D. *Adv. Mater.* **2010**, 22, 3032-3037.

(14) Lutkenhaus, J. L.; Hammond, P. T. *Soft Matter* **2007**, 3, 804-816.

(15) Liu, B.; Bazan, G. C. *Chem. Mater.* **2004**, 16, 4467-4476.

(16) Pinto, M. R.; Schanze, K. S. *Proc. Natl. Acad. Sci.* **2004**, 101, 7505-7510.

(17) Liu, B.; Bazan, G. C. *Proc. Natl. Acad. Sci.* **2005**, 102, 589-593.

(18) Duan, X. R.; Liu, L. B.; Feng, F. D. *Acc. Chem. Res.* **2010**, 43, 260-270.

(19) Duan, X. R.; Liu, L. B.; Feng, X. L. *Adv. Mater.* **2010**, 22, 1602-.

(20) Yang, G.; Yuan, H.; Zhu, C.; Liu, L.; Yang, Q.; Lv, F.; Wang, S. *ACS Appl. Mater. Interfaces* **2012**, 4, 2334-2337.

(21) Davies, M. L.; Douglas, P.; Burrows, H. D.; Martincigh, B.; Miguel, M. D.; Scherf, U.; Mallavia, R.; Douglas, A. *J. Phys. Chem. B* **2014**, 118, 460-469.

(22) Gaylord, B. S.; Heeger, A. J.; Bazan, G. C. *Proc. Natl. Acad. Sci.* **2002**, 99, 10954-10957.

(23) Al Attar, H. A.; Monkman, A. P. *J. Phys. Chem. B* **2007**, 111, 12418-12426.

(24) Monteserin, M.; Burrows, H. D.; Mallavia, R.; Di Paolo, R. E.; Maçanita, A. L.; Tapia, M. J. *Langmuir* **2010**, 26, 11705-11714.

(25) Åsberg, P.; Björk, P.; Höök, F.; Inganäs, O. *Langmuir* **2005**, 21, 7292-7298.

(26) Karlsson, K. F.; Åsberg, P.; Nilsson, K. P. R.; Inganäs, O. *Chem. Mater.* **2005**, 17, 4204-4211.

(27) Fonseca, S. M.; Galvão, R. P.; Burrows, H. D.; Gutacker, A.; Scherf, U.; Bazan, G. C. *Macrom. Rapid Comm.* **2013**, 34, 717-722.

(28) Toba, M.; Nakashima, T.; Kawai, T. *J. Polym Sci Part A: Polym Chem* **2011**, 498, 1895-1906.

(29) Ghoos, T.; Brasienne, J.; Fustin, C. A.; Gohy, J. F.; Defour, M.; Van den Brande, N.; Van Mele, B.; Lutsen, L.; Vanderzande, D. J.; Maes, W. *Polymer* **2013**, 54, 6293-6304.

(30) Ghoos, T.; Van den Brande, N.; Defour, M.; Brassinne, J.; Fustin, C.-A.; Gohy, J.-F.; Hoeppener, S.; Schubert, U. S.; Vanormelingen, W.; Lutsen, L.; Vanderzande, D. J.; Van Mele, B.; Maes, W. *Eur. Polym. J.* **2014**, 53, 206-214.

(31) Clément, S.; Tizit, A.; Desbief, S.; Mehdi, A.; De Winter, J.; Gerbaux, P.; Lazzaroni, R.; Boury, B. *J. Mater. Chem.* **2011**, 21, 2733-2739.

(32) Viinikanoja, A.; Areva, S.; Kocharova, N.; Ääritalo, T.; Vuorinen, M.; Savunen, A.; Kankare, J.; Lukkari, J. *Langmuir* **2006**, 22, 6078-6086.

(33) Ghoos, T.; Malinkiewicz, O.; Conings, B.; Lutsen, L.; Vanderzande, D. J.; Bolink, H. J.; Maes, W. *RCS Adv.* **2013**, 3, 25197-25203.

(34) Zilberberg, K.; Behrendt, A.; Kraft, M.; Scherf, U.; Riedl, T. *Org. Electron.* **2013**, 14, 951-957.

(35) Burns, C. T.; Lee, S.; Seifert, S.; Firestone, M. A. *Polym. Adv. Technol.* **2008**, 19, 1369-1382.

(36) Becht, G. A.; Lee, S.; Seifert, S.; Firestone, M. A. *J. Phys. Chem. B* **2010**, 114, 14703-14711.

(37) Lu, W.; Fadeev, A. G.; Qi, B. H.; Smela, E.; Mattes, B. R.; Ding, J.; Spinks, G. M.; Mazurkiewicz, J.; Zhou, D. Z.; Wallace, G. G.; MacFarlane, D. R.; Forsyth, S. A.; Forsyth, M. *Science* **2002**, 297, 983-987.

(38) Ho, H. A.; Bossinot, M.; Bergeron, M. G.; Corbeil, G.; Dore, K.; Boudreau, D.; Leclerc, M. *Angew. Chem. Int. Ed.* **2002**, 41, 1548-1551.

(39) Doré, K.; Dubus, S.; Ho, H.-A.; Lévesque, I.; Brunette, M.; Corbeil, G.; Boissinot, M.; Boivin, G.; Bergeron, M. G.; Boudreau, D.; Leclerc, M. *J. Am. Chem. Soc.* **2004**, 126, 4240-4244.

(40) Ho, H. A.; Doré, K.; Boissinot, M.; Bergeron, M. G.; Tanguay, R. M.; Boudreau, D.; Leclerc, M. *J. Am. Chem. Soc.* **2005**, 127, 12673-12676.

(41) Ho, H.-A.; Leclerc, M. *J. Am. Chem. Soc.* **2004**, 126, 1384-1387.

(42) Zheng, W.; He, L. *J. Am. Chem. Soc.* **2009**, 131, 3432-3433.

(43) Wang, L. X.; Bloomfield, V. A. *Macromolecules* **1991**, 24, 5791-5795.

(44) Borsali, R.; Nguyen, H.; Pecora, R. *Macromolecules* **1998**, 31, 1548-1555.

(45) Orberg, M. L.; Schillen, K.; Nylander, T. *Biomacromolecules* **2007**, 8, 1557-1563.

(46) Svergun, D. I.; Koch, M. H. J. *Rep. Prog. Phys.* **2003**, 66, 1735-1782.

(47) Putnam, C. D.; Hammel, M.; Hura, G. L.; Tainer, J. A. *Q. Rev. Biophys.* **2007**, 40, 191-285.

(48) Knaapila, M.; Evans, R. C.; Garamus, V. M.; Almásy, L.; Székely, N. K.; Gutacker, A.; Scherf, U.; Burrows, H. D. *Langmuir* **2010**, 26, 15634-15643.

(49) Evans, R. C.; Knaapila, M.; Willis-Fox, N.; Kraft, M.; Terry, A.; Burrows, H. D.; Scherf, U. *Langmuir* **2012**, 28, 12348-12356.

(50) Knaapila, M.; Evans, R. C.; Gutacker, A.; Garamus, V. M.; Székely, N. K.; Scherf, U.; Burrows, H. D. *Soft Matter* **2011**, 7, 6863-6872.

(51) Bondarev, D.; Zedník, J.; Šloufová, I.; Sharf, A.; Procházka, M.; Pfleger, J.; Vohlídal, J. *J. Polym. Sci. Part A: Polym. Chem.* **2010**, 48, 3073-3081.

(52) Blanton, T. N.; Barnes, C. L.; Lelental, M. *J. App. Cryst.* **2000**, 33, 172-173.

(53) Franke, D.; Kikhney, A. G.; Svergun, D. I. *Nucl. Instr. and Meth. in Phys. Res. A* **2012**, 689, 52-59.

(54) Svergun, D. I. *J. Appl. Cryst.* **1992**, 25, 495-503.

(55) Franke, D.; Svergun, D. I. *J. Appl. Cryst.* **2009**, 42, 342-346.

(56) Pedersen, J. S.; Schurtenberger, P. *J. Appl. Cryst.* **1996**, 29, 646-661.

(57) Prosa, T. J.; Winokur, M. J.; Moulton, J.; Smith, P.; Heeger, A. J. *Macromolecules* **1992**, 25, 4364-4372.

(58) Schmidt, P. W. *J. Appl. Cryst.* **1991**, 24, 414-435.

(59) Ying, Q.; Chu, B. *Macromolecules* **1987**, 20, 362-366.

(60) Mandelkern, M.; Elias, J. G.; Eden, D.; Crothers, D. M. *J. Mol. Biol.* **1981**, 152, 153-161.

(61) Ho, H.-A.; Najari, A.; Leclerc, M. *Acc. Chem. Res.* **2008**, 41, 168-178.

(62) Hwang, I.; Scholes, G. D. *Chem. Mater.* **2011**, 23, 610-620.

(63) Burrows, H. D.; Fonseca, S. M.; Silva, C. L.; Pais, A. A. C. C.; Tapia, M. J.; Pradhan, S.; Scherf, U. *Phys. Chem. Chem. Phys.* **2008**, 10, 4420-4428.

(64) Ferreira, B.; da Silva, P. F.; de Mello, J. S.; Pina, J.; Maçanita, A. *J. Phys. Chem. B* **2012**, 116, 2347-2355.

(65) Kewalramani, S.; Zwanikken, J. W.; Macfarlane, R. J.; Leung, C.-Y.; de la Cruz, M. O.; Mirkin, C. A.; Bedzyk, M. J. *ACS Nano* **2012**, 7, 11301-11309.

For Table of Contents use only

"Conjugated polyelectrolyte (CPE) poly{3-[6-(*N*-methylimidazolium)hexyl]-2,5-thiophene} complexed with DNA — Relation between colloidal level solution structure and chromic effects" by

Matti Knaapila, Telma Costa, Vasil M. Garamus, Mario Kraft, Ullrich Scherf and Hugh D. Burrows